MR SUSCEPTIBILITY WEIGHTED IMAGING

AND ITS CLINICAL APPLICATIONS

by

NANDITA RAMESH SHETTY

Presented to the Faculty of the Graduate School of

The University of Texas at Arlington in Partial Fulfillment

of the Requirements

for the Degree of

MASTER OF SCIENCE IN BIOMEDICAL ENGINEERING

THE UNIVERSITY OF TEXAS AT ARLINGTON

MAY 2006

ACKNOWLEDGEMENTS

The MR Susceptibility Weighted Imaging project was a roller coaster ride. It would be simple to list out the names of everyone who pitched in, but will be hard to thank them enough. This chapter could probably turn out to be the longest chapter and duly deserves to. I started this adventure not knowing anything except for some questions I had from the little reading I had done, which on day one triggered a series of mails from everyone involved. From then the on, the ball started rolling and continues to do so.

First of all, sincere thanks to my supervisor Dr. Michael D. Devous, Sr. I could not have imagined having a better mentor and advisor than him. I believe it was his perceptiveness, encouragement, assertiveness amongst other dynamic and brilliant qualities in him and knowing how to bring out the best in me which helped me complete my 'never ending' thesis. He had the answers to all my questions but would nevertheless force me to come up with my own solutions and force me to see the light at the other end of the tunnel every time we came across a dead end. He truly is an amalgamation of all the desired qualities one could ever ask for. Another pillar of motivation, an inexhaustible source of ideas and suggestions is Dr. Kaundinya Gopinath. He has been one of the greatest influences in my thesis. His sheer knowledge on MRI and his proficiency in the field encouraged me to read more and learn to appreciate the physics involved. He turned out to be an omnipresent guide who

immensely helped me turn ideas into reality. Dr. Roderick McColl was one of the very first professors I met at the University of Texas at Southwestern Medical Center and I was awestruck and fascinated by the infinite knowledge he possessed on my very first meet. He always had the answers to all the questions I had and I do hope that some day I too can reason out findings the way he does. Next Dr. Anthony Whittemore a neuroradiologist, some one who I always look forward to having a conversation with. I will probably never forget that one meeting of ours where he looked at me, smiled and said, "Where are you getting all these questions from? You don't even know how SWI would look like for a patient." He was the bridge between the technical and clinical world and helped make things tangible. I would forever bombard him with probable applications of SWI and seek his opinion on the same and he was always ready to hear me out irrespective of how impractical I could get. Dr. Richard Briggs was another dynamic personality I would constantly haunt. I used to take the liberty of barging into his office unannounced asking him about the sequence, magnet status etc. He has also been extremely accommodating, patient and kind enough to let me use the computer in his lab and treated me like one of his own students

Due credit also goes to Dr. Ramon Diaz Arrastia, Dr. Evelyn Babcock, Dr. Subhendra Sarkar, Carol Moore for their immense support and encouragement. Special mention goes to Dr. Khamid Bakhadirov who has been the backbone of the project. He partnered with me and continues to help spread the innumerable applications of SWI. On the same note I would like to thank Tom, Julie, Abhinay, Aman, Della, Jun Yi, Sina and the rest of the Nuclear Medicine group for their invaluable inputs. I consider myself

lucky to have a set of understanding, encouraging friends who were always there by my side and would patiently or rather was forced to listen to all the developments in my project whether they liked it or not apart from giving a deaf ear every time I said "I am never going to graduate".

Finally, this would not have been possible without the unlimited source of encouragement, motivation and faith of my family – Ramesh Shetty, Vijaya Shetty, Nitin, Nandana and Sachin hundreds of miles away from me. Sincere thanks again to my committee – Dr. Michael D. Devous, Sr., Dr. Richard Briggs and Dr. Hanli Liu for their interest in my work and for accommodating the last minute changes.

The preceding few lines of this chapter are sincere words of gratitude to everyone mentioned here. This has been a huge and tremendous learning experience and whatever I am today, will go on to be in the future is a consequence of my interaction and what I learnt from every one involved. I would like to extend my thanks and appreciation to them.

April 19, 2006

ABSTRACT

MR SUSCEPTIBILITY WEIGHTED IMAGING

AND ITS CLINICAL APPLICATIONS

Publication No. _____

Nandita Ramesh Shetty, MS

The University of Texas at Arlington, 2006

Supervising Professor: Dr. Michael D. Devous, Sr.

Susceptibility Weighted Imaging (SWI) is a new T2* weighted Gradient Echo sequence that exploits the magnetic properties of tissues due to local inhomogeneities in the magnetic field. This technique was originally called 'High-Resolution Blood oxygen level dependent Venography' which, as the name suggests provides an increased visibility of the venous vasculature in the brain, including the minute vessels not seen on conventional imaging techniques. Since its potential is not restricted to venography, it was renamed 'Susceptibility Weighted Imaging ' due to its contrast mechanism being the susceptibility differences between two tissues. The essential feature in this technique is to tap the paramagnetic properties, specifically those of the deoxygenated hemoglobin, in order to make deoxygenated hemoglobin

increasingly visible especially on the MRI phase images. To date, SWI is not a scanner derived image and remains to be a post-processed image reconstruction technique using various intermediate images (k-space, real and imaginary images). The processing techniques include filtering the phase data to remove the low frequency components in the background field, generation of a phase mask to enhance the susceptibility contrast seen in the phase images followed by multiplication of this phase mask with the magnitude images to make these phase variations prominent in the resultant susceptibility weighted image.

The study also emphasizes the clinical potentials of this high resolution imaging technique, particularly in the case of Diffuse Axonal Injury (DAI) in Traumatic Brain Injury. SWI holds clinical significance in the above mentioned pathology because studies proved that hemorrhagic lesions visible in SWI are significantly higher than those detected by conventional imaging techniques. These findings are primarily because susceptibility weighted imaging is capable of detecting microhemorrhages which are undetected in the case of CT scans and other current MR imaging techniques. This could help in SWI contributing to effective and efficient evaluation of DAI, bringing about a correlation between prognosis and outcome.

TABLE OF CONTENTS

Appendix

LIST OF ILLUSTRATIONS

Figure Page

LIST OF ABBREVIATIONS

AFNI …….	Analysis of Functional Neuro-Imaging
BOLD …….	Blood Oxygen Level Dependent
CT ……	Computed tomography
CV …….....	Control Variable
DAI …….	Diffuse Axonal injury
GRE …….	Gradient Echo
HRBV …….	High Resolution Blood oxygen level dependent Venography
ICH …….	Intra Cerebral Hemorrhage
mIP ……	minimum Intensity Projection
MR …….....	Magnetic Resonance
SWI …….	Susceptibility Weighted Imaging
TBI …….	Traumatic Brain Injury

CHAPTER 1

INTRODUCTION

1.1 Susceptibility Weighted Imaging

Susceptibility Weighted Imaging (SWI) is a new T2* weighted Gradient Echo technique that takes advantage of the magnetic susceptibility effects generated due to the local inhomogeneities in the magnetic field. This technique, developed by Dr. Mark Haacke, Dr. Reichenbach and their co-workers was originally called '**High-Resolution Blood oxygen level dependent Venography**' (HRBV) which, as the name suggests provides an increased visibility of the venous vasculature in the brain owing to its oxygenation level [1]. The essential feature here is to achieve high contrast between regions of different susceptibilities using the phase images along with its corresponding magnitude images. To date, Susceptibility Weighted Imaging is not a scanner-derived image and remains to be a post-processed reconstruction technique.

1.1.1 History and Overview

HRBV helps image veins of resolution up to less than a millimeter, by exploiting the BOLD (Blood Oxygen Level Dependent) induced phase effects which results in a signal cancellation between the venous blood and the surrounding brain parenchyma [2, 3]. This technique was developed to provide in depth information on

the venous vasculature in the brain. Owing to its potential applications in wide areas, it was coined '**Susceptibility Weighted Imaging**' due to its contrast mechanism being the susceptibility differences between two tissues. These unique susceptibility differences are more prominent in the phase images and thus, optimal visualization of the veins is achieved by superimposing the contrasts seen in these images on its equivalent magnitude images. With the correct sequence parameters, even minute venous vasculatures become increasingly visible. The SWI sequence is a strongly susceptibility-weighted, velocity-compensated, Gradient Echo (GRE) imaging sequence. The GRE sequence is preferred because these images are extremely sensitive, for they do not rephase the decay arising due to magnetic field inhomogeneities and magnetic susceptibility. Pauling et al. discovered the magnetic properties of blood in the fluid state and concluded that deoxyhemoglobin is paramagnetic while oxyhemoglobin is diamagnetic [4]. Studies have shown that voxels enclosing a mixture of paramagnetic and diamagnetic tissues will produce field variations at the interfaces due to the local susceptibility differences. These characteristics permit SWI to have exquisite sensitivity to veins, variations in iron content, blood products etc, owing to its susceptibility effects which results in a net loss of MR signal thereby helping delineate them from their surroundings.

1.1.2 Basic Principles underlying Susceptibility Weighted Contrast

'Susceptibility' is the property wherein a substance tends to get magnetized in the presence of a magnetic field. All materials have some level of magnetic susceptibility in them, be it paramagnetic or diamagnetic, which in turn is proportional

to the magnetic field [5]. When matter is subjected to an external field, electromagnetic interactions take place, which could result in the magnetic lines of force to either strengthen or weaken. This occurs due to the current generated from the action of the orbital and localized electrons within the matter in response to the magnetic field [6]. This circulating current tends to induce an internal magnetization within the matter. When the direction of this induced magnetization i.e. the alignment of the magnetic dipoles is in the same direction as the magnetic field, the effective field within the object is enhanced and when opposite, reduces the effective field. Paramagnetic substances demonstrate the former and have a positive magnetic susceptibility and tend to suppress the MR signal while *diamagnetic* substances exhibit the latter and have negative susceptibility [9]. Most proteins are diamagnetic while matter having unpaired electrons like deoxy-hemoglobin is paramagnetic. The greater the number of unpaired electrons, the greater is the paramagnetic effect.

Susceptibility Weighted Imaging makes use of the same principles. Technically when no matter is present, the magnetic induction or magnetic flux density (B) and the magnetic field intensity (H) is essentially equal [6]. But, in the presence of matter the applied field 'B' is not equal to the induced field 'H'. As explained earlier when the applied field encounters matter, there exists a circulating current and an induced internal magnetization (M) because of the unpaired orbital electrons. Mathematical relationships [1, 6] between 'B' and 'H' can be described for this phenomenon and is given by

$$B = \mu H \qquad (1.1.2\ a)$$

where,

B is the Magnetic flux Density (T or N/amp m)

H is the Magnetic Field Intensity (amp/m)

μ is the Permeability (N/amp^2);

$\mu = \mu_o \mu_r$ where,

μ_o is the permeability of free space ($4 * 10^{-7}$ N/amp^2)

μ_r is the relative permeability and is dimensionless

The relative permeability is > 1 for paramagnetic matter and < 1 for diamagnetic matter. From Maxwell's equation corresponding to Ampere's law, we get a mathematical definition [6] for the applied field, which obeys

$$H = \frac{B}{\mu_o - M} \qquad (1.1.2\ b)$$

where

H is the Magnetic Field Intensity (amp/m)

B is the Magnetic flux Density (T or N/amp m)

M is the internal magnetization (amp/m)

μ_o is the permeability of free space ($4 * 10^{-7}$ N/amp^2)

In the case of materials where the magnetization and applied field are proportional to each other, they can be described by a dimensionless quantity called the magnetic susceptibility (χ) [6], given by

$$M = \chi H \qquad (1.1.2\ c)$$

where

χ is the Magnetic Susceptibility

Comparing (1.1.2 b) and (1.1.2 c), we can obtain a relation between the magnetic susceptibility and the permeability [6], mathematically defined as

$$\chi = \frac{\mu_r}{\mu_o - 1} \quad \text{or} \quad \mu_r = \mu_o(1+\chi) \tag{1.1.2 d}$$

From (1.1.2 a to 1.1.2 d), we get

$$B = \frac{1+\chi}{\chi}\mu_o M(\chi) \tag{1.1.2 e}$$

From (1.1.2 d), we see that for diamagnetic substances the susceptibility is less than 0, while for paramagnetic substances the susceptibility is greater than 0. Non-magnetic materials have a susceptibility of 0. Any paramagnetic changes in the body quantized by '$\Delta\chi$' will increase the effective local field. Susceptibility variations are seen between 'heme' iron, 'non-heme' iron and at tissue interfaces. In SWI, the phase changes associated with these susceptibility effects are significant. Field changes due to variations in susceptibility results in a phase change [6] at the echo time TE, given by

$$\Delta\phi = -\gamma\Delta B(TE) \tag{1.1.2 f}$$

where,

$\Delta\phi$ is the change in phase (radians)

γ is the gyromagnetic ratio ($2.678 * 10^8$rad/s/T)

ΔB is the change in magnetic flux density (T or N/amp m)

TE is the time of echo (msec)

Also, $\Delta B = f(\Delta\chi)$ and from the above relationships, we see that there exists a unique change in phase with a change in magnetic susceptibility which is specific to the particular nuclei. One of the changes in magnetic susceptibility effects include reduction of the time constant T2* because of the dipole-dipole coupling of paramagnetic nuclei. This occurs due to the rapid dephasing of the voxels due to field inhomogeneities leading to a loss in MR signal. Thus, paramagnetic substances are seen as hypointensified regions in T2* and SWI images. There exists a phase change where the paramagnetic matter goes out of phase with its neighbors and this contrast is evidently conspicuous in the phase images. The reduction in T2* is given by the relationship [6]

$$\frac{1}{T2*} = \frac{1}{T2} + \gamma(\Delta B) \qquad (1.1.2\ g)$$

where,

T2* is the effective transverse relaxation time (msec)

T2 is the transverse relaxation time (msec)

As water photons diffuse across magnetically non uniform regions, they lose phase coherence which is proportional to the echo time which decreases the signal [13].

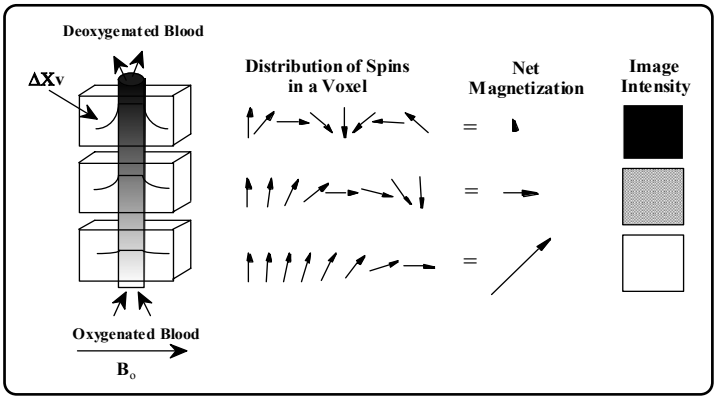

Figure 1.1 Illustration of the magnetic properties of Oxygenated and Deoxygenated blood [22]

1.1.3 Objects in External Fields: Infinite Cylindrical Body

Blood vessels can be modeled with the help of right circular cylinders of constant susceptibility.

Case (i) Cylinder parallel to the magnetic field

The changes in the magnetic field due to the presence of a cylinder parallel to the applied field are given by 'ΔB_{out}' and 'ΔB_{in}' where the former represents the resultant field outside the cylinder and the latter describes the resultant field inside the cylinder [6].

$$\Delta B_{out} = 0 \tag{1.1.3 a}$$

$$\Delta B_{in} = \chi B \tag{1.1.3 b}$$

Case (ii) Cylinder perpendicular to the magnetic field

The changes in the magnetic field due to the presence of a cylinder perpendicular to the applied field are given by 'ΔB_{out}' and 'ΔB_{in}' where the former represents the resultant field outside the cylinder and the latter describes the resultant field inside the cylinder [6].

$$\Delta B_{out} = \frac{\chi/2}{1+\chi/2}\left(\frac{\alpha}{\rho}\right)^2 Cos(2\phi)B \tag{1.1.3 c}$$

$$\Delta B_{in} = \frac{\chi/2}{1+\chi/2}B \tag{1.1.3 d}$$

where

ρ is a cylindrical coordinate defined such that ρ=0 is the cylinder axis

α is the radius of the cylinder

Case (iii) Cylinder inclined at an arbitrary angle to the magnetic field

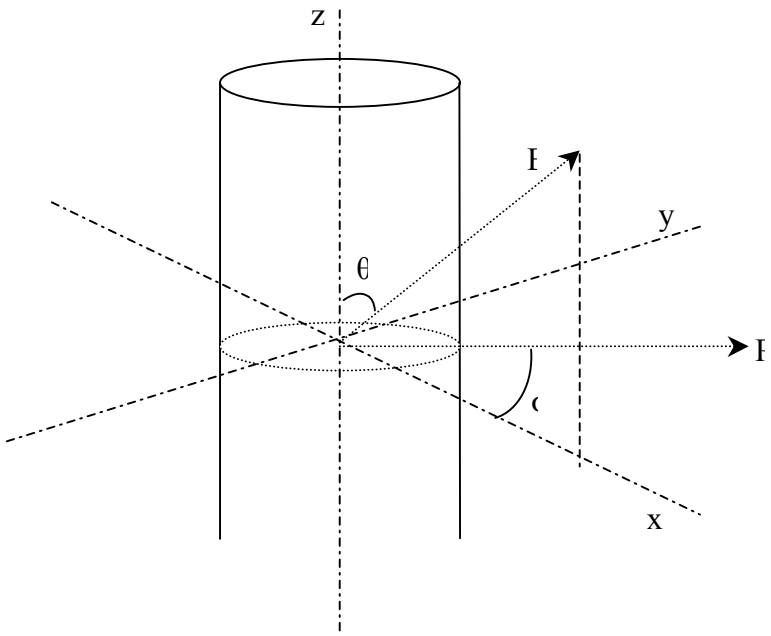

Figure 1.2 (ρ, Φ) describe the cylindrical coordinates describing the position P relative to the cylinder lying in the x-y plane at an angle θ to the external field [6].

The changes in the magnetic field due to the presence of a cylinder at an arbitrary angle 'θ' to the applied field are given by 'ΔB_{out}' and 'ΔB_{in}' where the former represents the resultant field outside the cylinder and the latter describes the resultant field inside the cylinder [6].

$$\Delta B_{out} \approx \left(\frac{\chi}{2}\right) B \left(\frac{\alpha}{\rho}\right)^2 \left(Sin^2\theta\right)\left(Cos2\phi\right) \qquad (1.1.3\ e)$$

$$\Delta B_{in} \approx \left(\frac{\chi}{2}\right) B \left(1 + Cos^2\theta\right) \qquad (1.1.3\ f)$$

where

(ρ, θ) is a cylindrical coordinates defined such that ρ = 0, θ = 0 is the cylinder axis

α is the radius of the cylinder

Φ is the polar angle in the x-y plane of the observation point given by $Tan^{-1}(y/x)$

Equations (1.1.3 e) and (1.1.3 f) assumes that the interface between two regions of varying susceptibility is sharp. In reality, a spin and its vicinity cannot be considered as a continuous distribution of magnetic field. In effect, the variation in the local field seen by a spin inside the cylinder is given by [1, 6, 8]

$$\Delta Bin \approx \left(\frac{\chi}{6}\right) B\left(3Cos^2\theta - 1\right) \qquad (1.1.3\ g)$$

1.1.4 Hemoglobin and its Susceptibility Effects

Hemoglobin is derived from the words '*heme'* meaning iron and '*globin'* which refers to its globular shape. The hemoglobin molecule is an assembly of four globular protein subunits, each subunit comprising of an iron atom [23]. Its primary function is that of being a blood oxygen transporter and can exist in two forms, **oxyhemoglobin** and **deoxyhemoglobin** which have different magnetic properties. In oxyhemoglobin as well as deoxyhemoglobin, the 'heme' (iron) is in the ferrous state [9]. When oxygen binds to the hemoglobin atom, there exists no free unpaired electron due to the covalent bonding (Fe^{2+}, two paired and four unpaired electrons). This makes the 'heme' iron in oxyhemoglobin diamagnetic like bulk water and cellular tissue. This iron has little effect on the relaxation times of water. On the other hand, when oxygen dissociates from the iron atom, it forms deoxyhemoglobin. This state of iron has 4 exposed, unpaired electrons and behaves like a tiny bar magnetic and so is paramagnetic in nature. Owing to its paramagnetic property, it induces an internal magnetic field that augments the magnetic field when placed in one.

Venous vasculature carry deoxygenated blood and thus is paramagnetic in nature. This acts as a source of susceptibility contrast owing to its magnetic properties. The local field induced by the magnetic susceptibility change in the venous blood causes the dephasing of the water signals (protons) of the blood and the surrounding tissue, say parenchyma. The magnetic field inhomogeneities caused due to this essentially results in two consequences:

- **Reduction of T2***

The paramagnetism results in the speeding of the transverse relaxation thereby reducing T2* i.e. reduces the relaxation rate of water which results in a loss of MR signal. Thus, a sufficiently long echo time will help differentiate veins from the rest of the tissues.

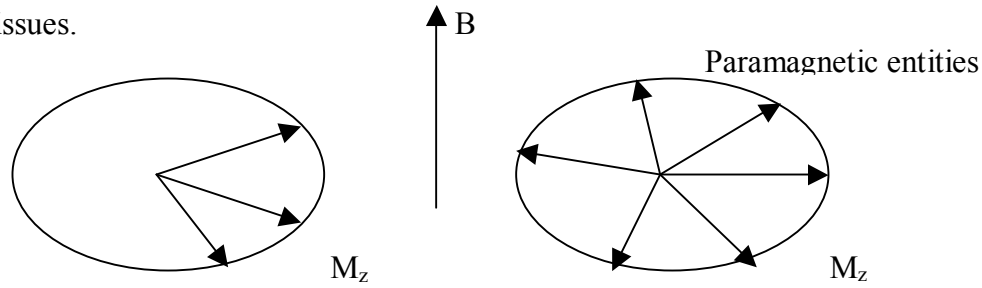

Figure 1.3 Illustrates the increased dephasing observed in paramagnetic matter. M_z represents the magnetization component.

- **Phase difference between the vessel and its surroundings or parenchyma**

The bulk susceptibility shift effect of deoxygenated blood results in a frequency shift of the protons which further leads to a phase shift between the protons and tissue spins. This results in the venous blood going out of phase with respect to the brain parenchyma, leading to a signal cancellation due to the partial volume effect between the two interfaces [10].

1.1.4.1 Two Compartment Model

Compartmentalization of paramagnetic species may be used to make clear the mechanism of venous visualization in Susceptibility Weighted Imaging. Consider a voxel that encloses a single vein. From equation (1.1.3 g), one can presume that in the presence of a background tissue with 'χ_i' and 'χ_e' representing the susceptibility inside and outside the vessel, the net magnetic field shift is given by [1, 6, 8]

$$\Delta B_{in} \approx \left(\frac{\Delta\chi}{6}\right) B\left(3Cos^2\theta - 1\right) \qquad (1.1.4.1\ a)$$

where

ΔB_{in} is the field shift inside the venous vessel (T or N/amp m)

$\Delta\chi$ is the susceptibility shift given by χ_i-χ_e

B is the applied magnetic field (T or N/amp m)

θ is the angle extended by the vein with respect to the filed

Susceptibility of the blood system in general is given by

$$\chi_{blood} = Hct\left(Y\chi_{oxy} + (1-Y)\chi_{deoxy}\right) + (1-Hct)\chi_{plasma} \qquad (1.1.4.1\ b)$$

where χ_{blood} , χ_{oxy} , χ_{deoxy} , χ_{plasma} represents the magnetic susceptibility for the whole blood, oxygenated blood, deoxygenated blood and plasma respectively [1, 6, 8].

Hct is the hematocrit which is the fraction of the volume of packed red blood cells to the volume of whole blood. It is typically about 40% to 46% i.e. 0.40 to 0.46

Y is the oxygenation level which describes the fractional oxygenation in red blood cells and is 0.55 in accordance to the results of Weisskoff et al. It typically ranges from 0 to 1

Any change in the oxygenation level alters the susceptibility which can be represented as [6]

$$\Delta\chi_{blood} = -\Delta Y\left(\chi_{deoxy} - \chi_{oxy}\right)Hct \qquad (1.1.4.1\ c)$$

This difference in susceptibility between fully oxygenated and deoxygenated blood is given by

$$\chi_{do} = \chi_{deoxy} - \chi_{oxy} \qquad (1.1.4.1\ d)$$

Weisskoff et al. calculated susceptibility difference value 'χ_{do}' to be (4Π x 0.18ppm) per unit Hct. Studies indicate that oxygenated blood more or less have the same susceptibility as the surrounding tissue, which means 'χ_{oxy}' is equal to 'χ_{tissue}'.

Equation (1.1.4.1 b) now becomes [1, 6, 8]

$$\Delta\chi_{blood,tissue} = 4\pi(0.18)Hct(1-Y) \qquad (1.1.4.1\ e)$$

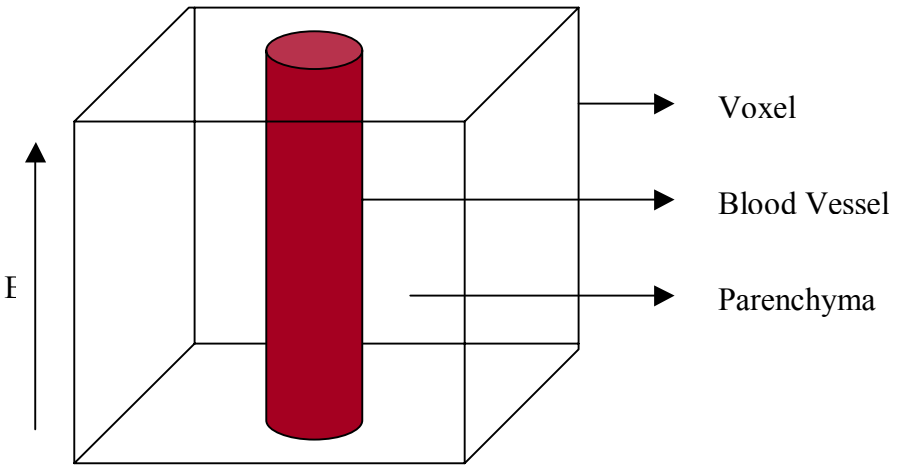

Figure 1.4 The two compartment model: the voxel comprises of a single venous blood vessel and parenchyma tissue [8].

In the two compartment model as illustrated in Figure 1.4, assume the vessel to be parallel with respect to the applied magnetic field. Owing to its orientation, there exists

no extravascular field effect. From equation (1.1.2 f), the change in phase between the venous and surrounding parenchymal tissue spins [1, 6, 8] is given by

$$\phi = -\gamma \Delta B(TE) \qquad \text{(1.1.4.1 b)}$$

where

γ is the gyromagnetic ratio for photons ($2.678 * 10^8$ rad/s/T)

ΔB is the field difference between the blood and parenchyma (T or N/amp m)

TE is the time of echo (msec)

Φ is the phase (radians)

From equation (1.1.4.1 c), substituting 'θ' with zero because of the vein being parallel to the field [1, 6, 8], we get

$$\Delta B = 4\pi(0.18)Hct(1-Y)B \qquad \text{(1.1.4.1 c)}$$

Calculating and substituting for 'ΔB' in equation (1.1.4.1 b) for a 3T scanner and substituting the gyromagnetic ratio, the phase difference between the venous blood and brain parenchyma is approximated [1, 6, 8] by

$$\phi = -40\pi(TE) \qquad \text{(1.1.4.1 d)}$$

It is evident that for a TE of 25msec, the phase becomes equal to -$\prod$ proving that the venous blood is out of phase with respect to the surrounding parenchyma. Here, the voxel containing the vein and background tissue (parenchyma) represents a bicompartment model, and there exists partial voluming of the two. Now, the venous blood signal will oppose that of the background tissue and will result in maximum signal cancellation leading to reductions in the MR signal. It is this behavior of the bicompartment model which allows venous vasculature of minuscule diameter to

become apparent in the susceptibility weighted images. Also, signal cancellation depends on the fraction of the signal that arises from two compartments. Maximum cancellation is obtained when the venous signal fraction is equal to 50% of the signal of the voxel [1, 6, 8].

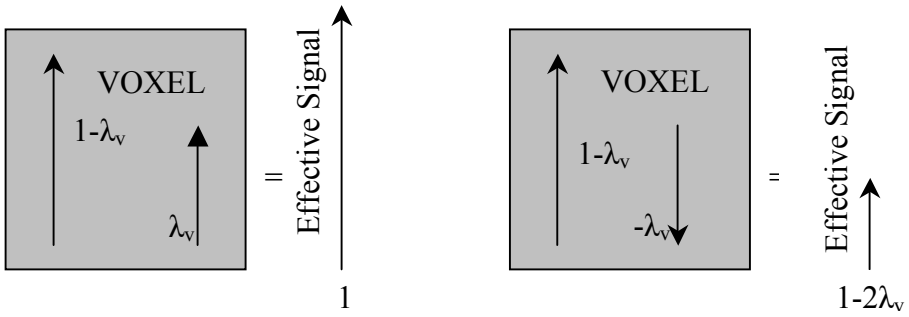

Figure 1.5 Illustration of the effects of venous signal partially canceling that of the surrounding tissue in the voxel. Assume that the parenchyma has a volume fraction $1-\lambda_v$ and the venous blood has a volume fraction of λ_v. If there were no phase effect, the sum of these two terms would yield unity. By selecting an appropriate TE, the signal from the vein can be inverted to go out of phase with the surrounding tissue. This results in a net signal loss [1, 6, 8].

As derived in equations (1.1.3 e) and (1.1.3 g), when the venous vessel is oriented at an arbitrary angle 'θ' with respect to the main field, there exists an intravascular field proportional to $(3\text{Cos}^2\theta - 1)$ and an extravascular field that is proportional to $(\sin^2\theta\ \text{Cos}^2\varphi/r^2)$. This extravascular field itself leads to signal cancellation. These vessels have a natural signal loss associated with their orientation. For vessels perpendicular to the field, the phase from inside the vessel becomes positive, but for small vessels, the phase from the tissue outside the vessel dominates, leading yet again to an effective negative and detectable phase [1, 6, 8]. These intravascular and extravascular signal losses make it possible to visualize vessels with diameters as minute as a few hundred micrometers which are embedded in voxels with

sizes of the order of $1mm^3$ [4,10]. Thus, susceptibility weighted imaging proves to be a more powerful and sensitive imaging technique.

1.2 Image Reconstruction Technique

Susceptibility Weighted Imaging is a new imaging sequence and remains to be a post processing technique using the intermediate images generated by the scanner. The SWI sequence is a fully velocity-compensated, Gradient Echo (GRE) sequence acquired typically with a conventional circularly-polarized head coil and requires separate acquisitions of phase and magnitude data or real and imaginary images which are the raw images generated by the scanner. It also requires an appropriate TE.

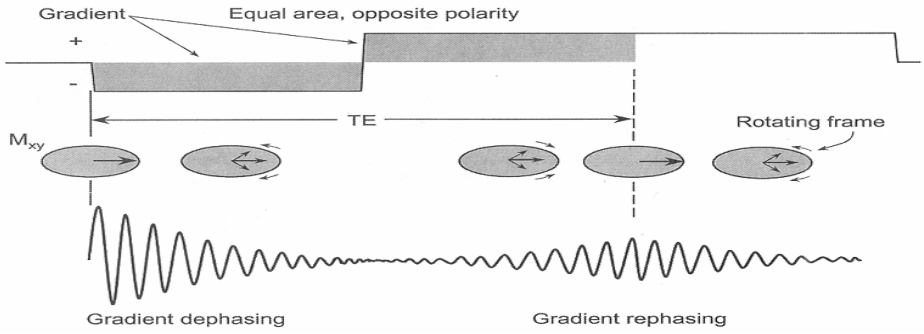

Figure 1.6 Illustration of the Gradient Echo Sequence which incorporates an RF dephasing pulse and a refocusing gradient reversal [22].

The post processing effectively enhances the signal losses caused by the paramagnetic tissues (areas that have iron) thereby making them more discernable. As mentioned before, the contrasts which arise due to the susceptibility effects are more prominent in the phase images. These phase images tend to represent the differences in local precession frequencies which in turn depend on the bulk susceptibility of the different tissues types or different blood oxygenation levels which are the sources of

signal contrasts [14]. Thus, the goal of the post processing technique is to make these hypointensity contrasts in the phase images significantly apparent on the magnitude images for better visualization. The steps generally involve filtering of the k-space data to remove aliasing artifacts, generation of a negative phase mask to take advantage of the negative phases that manifest which represents the iron laden tissues and finally the multiplication of this normalized magnified (to maximize the negative intensities) phase mask with the magnitude images. Thus, phase images of the brain can extensively compliment the magnitude images and further enhance the differentiation between tissues of varying magnetism.

1.3 Clinical Applications

Susceptibility Weighted Imaging is highly sensitive not only to the oxygen concentration of the intravascular blood but also to its break down products and other paramagnetic entities [3]. This makes SWI eligible to help diagnose various clinical conditions. At present, its application includes stroke and Diffuse Axonal Injury in Traumatic Brain Injury patients. It is being considered as a promising technique to help evaluate neurological trauma, brain neoplasm and neurovascular diseases owing to its ability to reveal vascular abnormalities and microbleeds which are not detected by conventional MR imaging techniques as well as modalities [12].

1.4 Objective

The objective of the thesis was to reconstruct the Susceptibility Weighted Images from the raw scanner images and to emphasize its potential applications owing to the high visibility of venous vasculature and other paramagnetic elements. Another

aim was to exploit the principles of SWI to detect microhemorrhages in DAI patients in Traumatic Brain Injury to help in an efficient and effective evaluation of the same. Currently, there exists no significant correlation between prognosis and outcome. This is because microhemorrhages are undetected in conventional imaging techniques and are not accounted for. SWI is thus proposed to benefit in better diagnosis and treatment planning of DAI.

CHAPTER 2

METHODS

2.1 Introduction

This chapter describes the SWI sequence and the various post-processing techniques required for the reconstruction of the images. The algorithm involves careful manipulation of the raw images generated by the scanner. These raw images include the real, imaginary and magnitude images which are acquired after specific settings on the MR acquisition console. The reconstruction algorithm was written in MATLAB (Version 7.0.2).

2.2 Image Reconstruction

A diagrammatic representation of the image processing techniques is as follows:

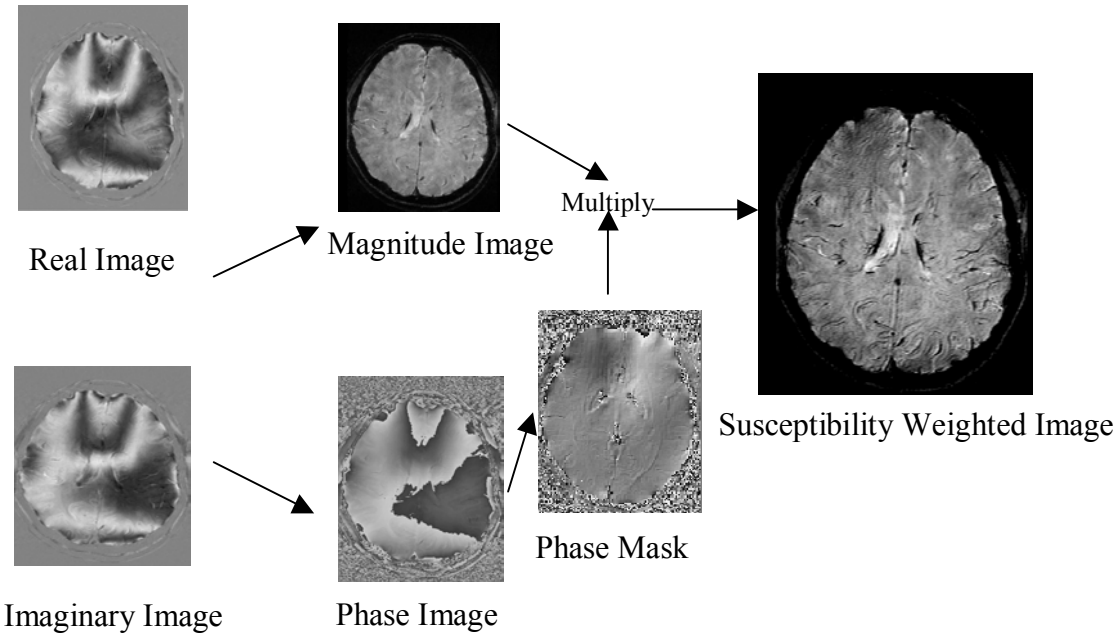

Figure 2.1 Illustration of the processing steps involved in the reconstruction of SWI

2.2.1 Data Set

The study involves the data set of two normal controls, one scanned with the 8 channel phased array coil while the other was scanned using a circular polarized quadrature coil.

2.2.2 MR Sequence and Acquisition

The MRI sequence is key to tapping the susceptibility contrasts and obtaining good end images. The subjects were scanned using the 3T GE Medical Systems Scanner at Meadows Imaging Center at the University of Texas Southwestern Medical Center at Dallas. The SWI examination was performed with the quadrature head coil as well as the 8 channel phased array coil. The sequence is a first order flow-compensated gradient echo sequence with a TR of 58ms, TE of 40ms and a flip angle of 20^0. The resolution maintained was (0.39 x 0.39 x 2.5). GRE sequences demonstrate the highest sensitivity to variations in susceptibility. The GRE is a preferred sequence because the signal is generated by the reversal of the read out gradient. It does not require the refocusing phase reversal pulse. This results in the preservation of the magnetic field gradients that are not compensated for and will result in signal attenuation. Also, the dephasing of the signal produces a signal void in the image that is larger than the physical volume of the tissue and this enables one to view minute vessels as well which are not detectable in conventional imaging techniques. In all, 56 slices each 2.5mm thick were acquired. The SWI sequence implemented was not an optimized sequence but, was nevertheless used to test the efficiency of the image reconstruction algorithm. SWI requires saving the real, imaginary, phase as well as the magnitude images. The intermediate images are

obtained on getting in to the Research Mode by setting the patient ID to '*geservice*'. To get images apart from the magnitude images, we need to modify the Control Variable (CV) to '*rhrcctrl*'. This is a bit mask, with the default value set to 1 which enables one to capture the magnitude images. The corresponding bitmap values for the real, imaginary and phase are 4, 8 and 2 respectively. So, in order to obtain the real, imaginary, phase and magnitude images we need to set the bit mask value to 1+4+2+8. The flip angle was set at 20^0 to avoid nulling the signal from the cerebral spinal fluid and pial veins and also to obey the bicompartment model. It also results in a lower energy being imparted to the tissues. The TE was set to 40ms. To avoid phase aliasing, a judicious choice of TE is to be made [12]. The subject was scanned without administering any intra venous paramagnetic contrast agents. The scan in all took about 8 minutes.

2.2.3 Image Pre-processing Steps

The image reconstruction algorithm was developed in MATLAB and takes about 8.5 min to construct 56 slices. The inputs to the program are the real, imaginary and magnitude images. All images were in DICOM format.

2.2.3.1 High Pass Filtering of Images

The static background field inhomogeneities are sources to low, spatial frequency components within the image. A high pass filter is implemented to filter out these variations. It involves two steps. In the first step, a 2D low pass Hanning filter is implemented on the original k space data. The filter smoothens out the phase variations, helps in phase unwrapping to a certain extent and also extracts the main spatial behavior

of the field. The filter sizes of the mask were varied from 3,6,8,32,64 to determine the best results. Desired images were produced for lower mask sizes. Care must be taken to not keep a very high filter size for this could result in extensive smoothing of the image and could smudge the minute vessels in the phase images. The second step involves dividing the complex image data with the filtered image data.

A thorough explanation of the filtering process is as follows. The MR complex signal consists of components from both the back ground static filed and the field differences induced by the paramagnetic deoxyhemoglobin [1, 15]. This signal is constructed using the real and imaginary images acquired from the scanner. The Fourier transform of this complex image gives us the k space data. The complex image can be mathematically defined by

$$\rho_o(x) = |\rho_o(x)| e^{i\varphi_f(x) + i\varphi_v(x)} \qquad \text{(2.2.3.1 a)}$$

where

$\rho_o(x)$ is the complex data in the spatial domain

$\varphi_f(x)$ is the phase component from the local field inhomogeneities

$\varphi_v(x)$ is the phase component from the venous blood

Lower frequency components of the k space which correspond to the center region of the k space image contain the inhomogeneities due to the static field [15, 20, 21]. To extract this behavior, the k space data is filtered using a Hanning filter and is given by

$$\rho_h(x) = |\rho_o(x)| e^{i\varphi_f(x)} = F^{-1}[S(k)H(k)] \qquad \text{(2.2.3.1 b)}$$

where

$\rho_h(x)$ is the low pass filtered complex data in the spatial domain

S(k) is the k space data in the frequency domain

H(k) is the n point k space filter in frequency domain

From the above equation (2.2.3.1 b), we see that we have only that component of the complex signal which contributes to the low spatial frequency phase variations. The next step involves the complex division of the original image with the low pass filtered k space data which essentially gives us the filtered image $\rho_f(x)$ [15, 20, 21].

$$p_f(x) = \frac{|\rho(x)|e^{i\varphi_f(x)+i\varphi_v(x)}}{|\rho_o(x)|e^{i\varphi_f(x)}} = |\rho_f(x)|e^{i\varphi_v(x)} \qquad (2.2.3.1\ c)$$

Equation (2.2.3.1 c) confirms that an effectively high pass filtered image has been obtained, thereby suppressing the background inhomogeneities and make prominent the venous vasculature.

2.2.3.2 Generation of Phase Masks

In the filtered phase images, the arteries and muscles have small positive phase values while the veins appear dark owing to their susceptibility differences [15, 20, 21]. These images have their values ranging from – Π to + Π. A phase mask is created which will be used to multiply with the magnitude image to make prominent the venous vasculature. This mask is constructed to enhance pixels of interest and suppress pixels of certain phase values. As mentioned earlier, the venous vasculature goes out of phase with the parenchyma and appears dark on the phase images as hypointensified regions. Hence, our pixels of interest are those ranging from – Π to 0 and so a **negative phase**

mask is generated. If the minimum phase of interest is – Π, then the phase mask is designed such that values of phase ranging from 0 to Π are set to unity while phase values less than 0 were normalized from 0 to 1. The phase mask [15, 20, 21] is constructed using

$$f(x) = \frac{\varphi(x) + \pi}{\pi} \text{ , for } \varphi(x) < 0$$

$$f(x) = 1 \qquad \text{otherwise} \qquad (2.2.3.2 \text{ a})$$

where,

f(x) is the phase mask which assumes values from 0 to 1

φ(x) is the phase value at location x in the filtered phase images

The above mask completely suppresses phase values of –Π and values ranging from 0 to – Π are partly suppressed.

2.2.3.3 Phase Mask Multiplication and Construction of SWI

Phase masks are designed to boost the contrast in the magnitude images. The phase mask can be applied any number of times to the magnitude image. Depending on the filter size and the TE value, the number of multiplications needed to optimize the contrast in the Susceptibility Weighted is determined. The number of multiplications normally ranges from 2 to 8. If the TE is set to a shorter interval, then more multiplications are required. The Susceptibility Weighted Image is processed after multiplying the normalized phase mask [15, 20, 21] with its corresponding magnitude image given by

$$\rho_{new}(x) = f^{m}(x)\rho(x) \qquad (2.2.3.3 \text{ a})$$

where

m is the number of times the mask is multiplied

f(x) is the normalized phase mask

ρ(x) is the corresponding magnitude image

This multiplication results in the generation of the Susceptibility weighted Images wherein the venous vasculature which is more prominent in the phase images to be reflected on the magnitude images. Since the phase mask used is a negative phase mask, the hypointensified pixels are more intense based on the number of multiplications.

2.2.4 Image Post-processing Steps – Minimum Intensity Projection (mIP)

The Susceptibility Weighted Images are high resolution images which depict venous vasculature to a resolution of less $5mm^3$ which are not visible on conventional imaging techniques. The venous vasculature appears as hypointensified regions in the brain. For better visualization of the same, a minimum intensity projection is performed on the SWI. This results in the veins to appear more tubular in nature which helps in easy identification and better visualization. Minimum Intensity Projection (mIP) is a post processing technique which projects the minimum intensities found along the projection ray in a slice. In the case of SWI, contiguous slices are mIPped to get SWI images which makes the vasculature look more real owing to its tubular appearance. The SWI images were mIPped to produce 2 data sets, one where the number of slices collapsed were 4 and another where the number of slices collapsed was 6. This can help delineate vasculature from other structures like lesions, tumor etc.

The minimum intensity projection was performed in AFNI on a LINUX platform. The SWI images were saved in raw format in MATLAB and were converted to the AFNI BRIK and HEAD files using the to3d command on the LINUX terminal. These images were opened in the AFNI viewer. On clicking the *DISP* menu, the *projection* menu is chosen which a drop down list box is. *Min* is selected in order to perform the Minimum Intensity Projection and the number of slices to be collapsed is chosen by changing the options in the *Slab* menu. The final mIPped images were saved for perusal.

CHAPTER 3

RESULTS AND DISCUSSION

3.1 Results

The objective of the thesis was to develop an algorithm to reconstruct the Susceptibility Weighted Images, emphasize its clinical applications and to test its efficiency particularly in evaluating DAI in the traumatic brain injured patients.

The SWI images were successfully reconstructed for the given sequence. The scans were performed on the 3T GE scanner. It must be noted that the sequence implemented was not an optimized one. The variables in the algorithm which need to be tweaked according to the SWI images obtained (which are dependent on the sequence and coil used) are the 'filter mask size' and the 'phase mask multiplication factor'. As far as assessing DAI patients using SWI, the analysis could not be done because no patient data sets could be obtained.

3.1.1 Reconstruction of k space data from the real and imaginary images

The SWI sequence was implemented using the quadrature coil as well as the 8 channel phased array coil. The reconstruction algorithm requires the k space image. This could either be constructed using the real and imaginary images or the phase and magnitude images. Successful reconstruction was possible using the quadrature coil but the k space data could not be generated from the phased array coil, because the real and imaginary images generated are calculated as the sum of the squares of each coil

element. This resulted in a scaling effect due to the coil acquisition technique. The k space data could have also been constructed using the magnitude and phase images but these phase images were in radians and scaled to 1000. Hence the phase values did not range from –Π to +Π and also the transformation function information was not available and so could not be corrected for. The data set from the 8 channel phased array coil was not processed further.

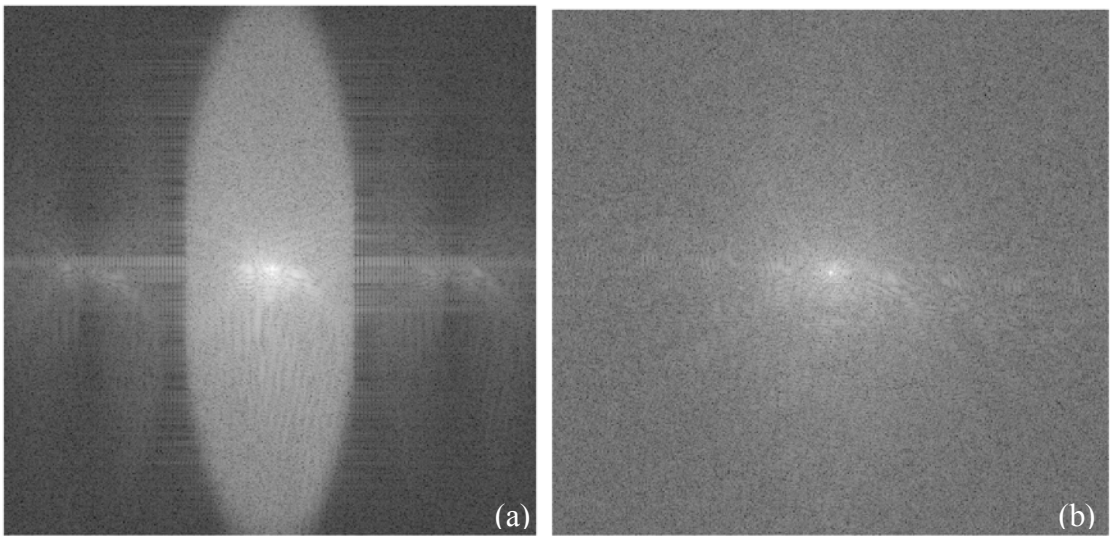

Figure 3.1 The k space image constructed from the real and imaginary images of the controls on the 3TGEMS (a) 8 channel phased array coil (b) Quadrature coil.

3.1.2 High Pass Filtering

As mentioned earlier, the low pass Hanning filter mask was varied to find the order which gave the best results. It was seen that a mask size of 8*8 for the low pass filter produced the best results for the data sets in hand. The mask size was set to that value which resulted in homogeneous phase images, thereby generating superior Susceptibility Weighted Images. However, literature suggested that a mask size of 64*64 works the best. This did not work with the data set under consideration because

of the susceptibility artifacts generated due to multiple dental fillings in the subject. While, 64*64 shows excellent contrast between gray matter, white matter and venous vessels, it did not produce a homogeneous phase image after the effective high pass filtering. This was because the susceptibility artifact was not smoothened out completely as illustrated in Fig 3.2 (d).

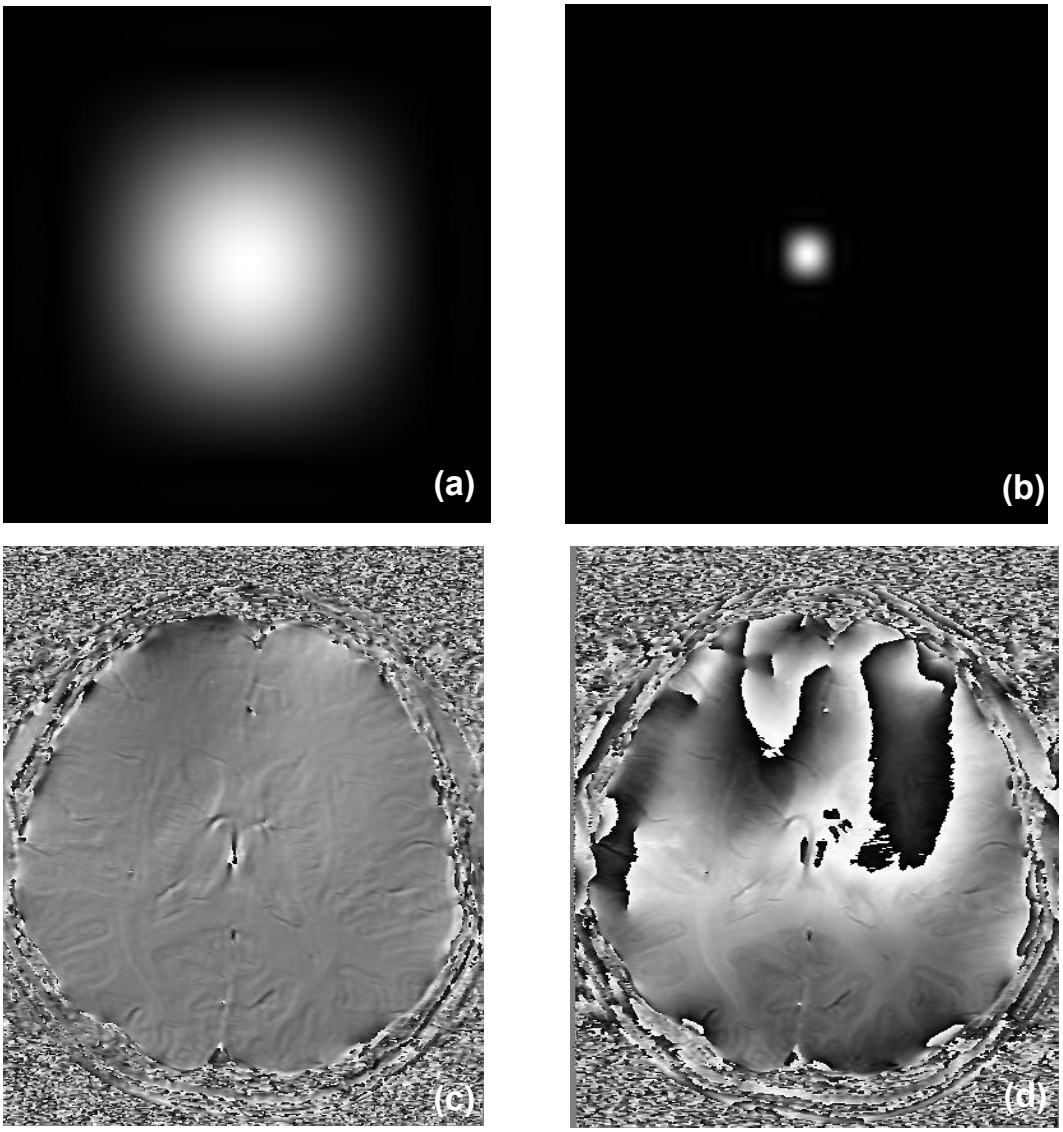

Figure 3.2 (a, b) The (8x8), (64x64) low pass Hanning Filter in frequency domain. (c, d) represents the corresponding high pass filtered phase image.

3.1.3 Susceptibility Weighted Images

56 SWI slices were produced from the corresponding real, imaginary and magnitude data set. The multiplication factor for the phase mask was varied from 2 to 8 with 6 being the optimum value. It can be clearly seen in Fig 3.3 (c,d) that the venous vasculature is more prominent in these resultant SWI images as opposed to the original magnitude images which proves the merit of this imaging technique.

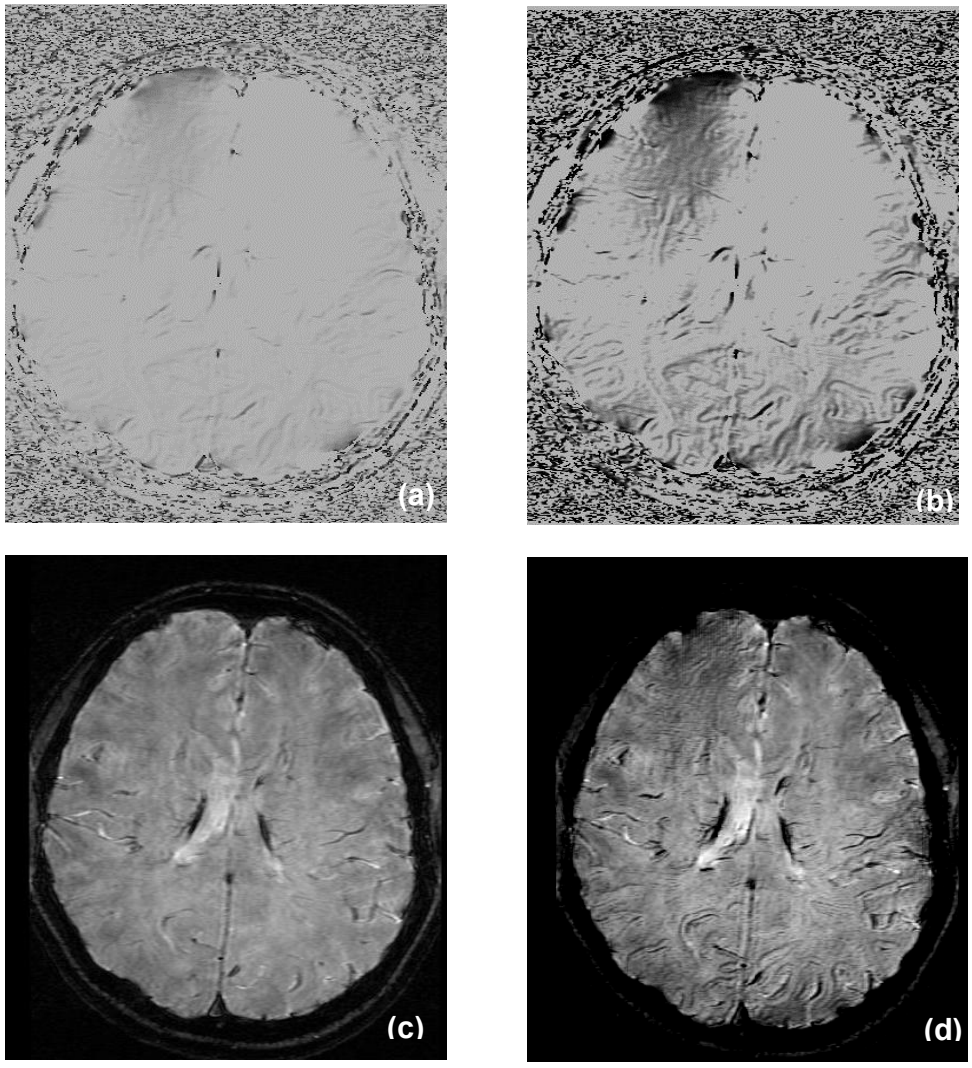

Figure 3.3 (a, b) The phase mask with a multiplication factor of 4 and 6 (c) Magnitude Image-Slice 34 (d) Corresponding SWI, Slice 34 with a multiplication factor of 6

3.1.4 Minimum Intensity Projection

Minimum Intensity Projections were performed on AFNI where 4, 6 and 10 contiguous slices were collapsed to form a single slice. Once done, the minimum intensities of pixels in the collapsed slices are extracted and displayed on a single slice. The vasculature now assumes a tubular appearance and looks more 'vessel' like. This helps in differentiating them from other hypointensified structures. Good end images were obtained after mIPping 4 and 6 SWI slices as shown below.

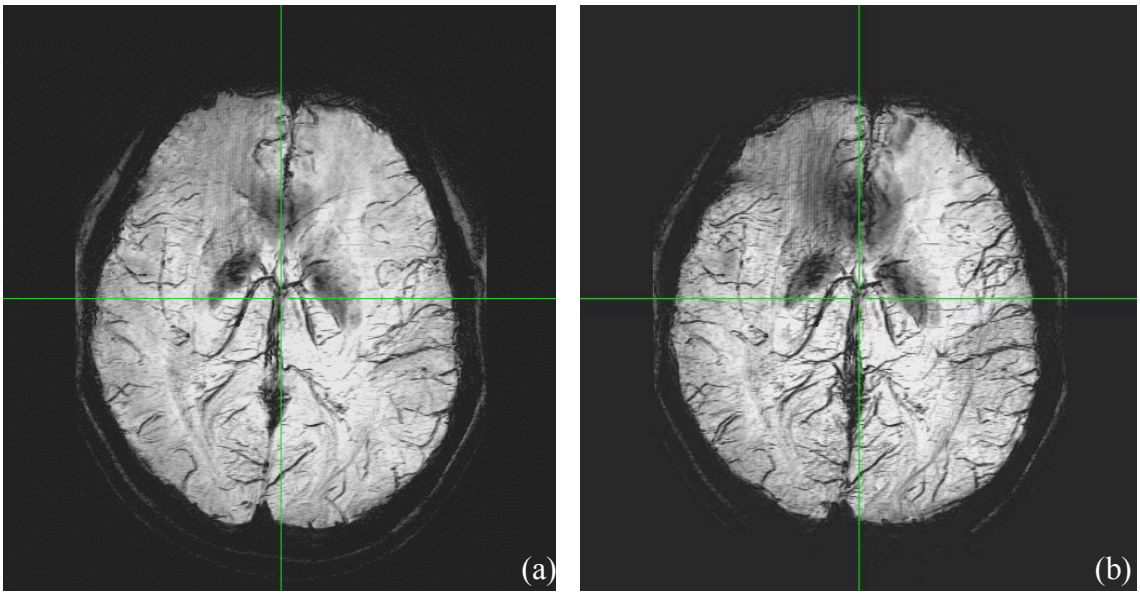

Figure 3.4 (a) and (b) represent the mIPped image of 4 and 6 SWI slices

3.2 Discussion

Susceptibility Weighted Imaging is a new imaging technique and has tremendous applications. The results obtained were reasonably good in spite of not having the right sequence. The reconstruction algorithm was written in MATLAB 7.0.4 and took 8.5 min of processing time to generate 56 SWI slices.

The reconstructed SWI images had artifacts on the upper right side of the image. These artifacts are manifested as hypointensified regions and were more prominent on the phase images and were discovered to have been caused due to multiple dental fillings in the control subject. Owing to the paramagnetic nature of these fillings, susceptibility artifacts were seen on the images. This artifact could not be corrected for owing to its hypointensified nature. Unfortunately, this limited any further statistical analysis of the SWI images in terms of histogram etc, because these artifacts were hypointensified pixels and as far as SWI is concerned, the hypointensified pixels also indicated the venous vasculature.

As far as the algorithm is concerned, it was observed that, smaller mask sizes for the low pass Hanning filter resulted in the filtered phase images being more homogeneous, but sharpness of the image reduced. The ideal filter size was chosen to be 8x8 to compensate for the susceptibility artifacts after different trials of mask size. The only other variable in the program is the phase mask multiplication factor. This reconstruction algorithm was tested for multiplication factors from 2 to 8. To reduce the scan time, TE could be reduced. The compensation for this would be to increase the number of multiplication factors to obtain equally good visibility of the venous vessels [1, 5, 19]. For the sequence under consideration, the TE was set at 40msec the mask size at 8x8 and multiplication factor at 6. The mIPped images help clearly distinguish the vasculature from other hypointensified entities. Also, for lesion studies this could prove useful to count the number of lesions. In some cases lesions might extend over two

slices. Without mIPping the images, this could result in the same lesion being counted twice and could result in a wrong treatment plan.

It must be taken into consideration here that the TE value chosen was probably not right. According to the bicompartment model, it should have been around 20msec. The downside of a high TE results in unnecessary phase wraps resulting in minute vessels not being detected.

Reconstruction of the Susceptibility Weighted Images requires the raw images to be in its original/pure form. Any form of scaling or transformation could result in phase wraps and this could hamper the opportunity of detecting the phase changes caused due to the susceptibility differences in the tissue. It was observed that the 8 channel phased array coil reconstructed real and imaginary images in a not so straightforward manner. Complicated techniques are involved because Free Induction Decay signals are acquired from each channel in the coil. Thus, k space data was not realized successfully. The circular polarized coil on the other hand is more simplistic in generating real and imaginary images. The disadvantage of circular polarized coil over phased array coil is that a better signal to noise ratio is obtained from the latter.

Susceptibility Weighted Imaging displays its superiority owing to its inherent ability to detect paramagnetic entities that are even miniscule in nature. The partial volume effect results in detection of entities almost 4 times smaller than the voxel size. The voxel size chosen for the sequence was (0.39 x 0.39 x 2.5). Thus, if images are acquired at a high resolution, one would get excellent clarity as far as the paramagnetic structures are concerned.

Due to inevitable circumstances, no data sets for DAI patients were obtained. This limited the opportunity to evaluate the potential of SWI in DAI. But, nevertheless one can claim from resultant SWI images obtained, that it indeed could help in detecting microhemorrhages.

3.3 Clinical Applications of SWI

Susceptibility Weighted Images are exquisitely sensitive to the venous vessels, blood products, iron laden tissues as well as changes in iron content [1, 5, 8]. These characteristics make it ideal to help evaluate and diagnose various pathological conditions. Major areas of its clinical applications today include cerebral stroke and Diffuse Axonal Injury (DAI) in Traumatic Brain Injury patients (TBI).

3.3.1 Diffuse Axonal Injury

Diffuse Axonal Injury (DAI) is known to be the common mechanism of injury in approximately 40% to 50% of Traumatic Brain Injury cases in the United States and derives its name because of the "diffuse damage of the cerebral white matter" caused [3, 5]. DAI is believed to be the most common cause of post-traumatic coma and vegetative state, and also is responsible for most neurological and neuropsychological impairments. Pathologically, it results in the tearing of axonal fibers due to shearing forces during acceleration, deceleration and rotation of the brain. The degree of insult depends on the magnitude of the force and the rate of deceleration associated with the tissue. Predominant locations of DAI include the hemispheric subcortical lobar white matter, centrum semiovale, corpus callosum, vassal ganglia, cerebellum and brain stem [2]. DAI is manifested as hemorrhagic and non-hemorrhagic lesions, with the latter

being more common. These lesions vary in shape and size, though are usually ovoid with their long axis parallel to the direction of the involved axonal tracts and range from 1mm to 15mm. Gennarelli et al. suggested three grades of DAI. Grade I involves non specific axonal damage without focal abnormalities, in grade II exists Grade I along with focal abnormalities especially in the Corpus Callosum and is most often associated with small tissue tear hemorrhages. Grade III assumes level I and II, with the addition of rostral brain stem injury [3].

Conventional imaging techniques like the CT scan or other MRI sequences fail to detect microhemorrhages which result in false negatives and leading to misdiagnosis and treatment which in some cases could prove fatal to the patient. This leads to DAI not being well characterized and often correlates with poor outcome, i.e. there exists poor correlation between prognosis and outcome. Thus, there arises a necessity to come up with a potent imaging technique that can detect these minute hemorrhages. SWI, owing to its sensitivity to venous blood and its break down products could prove to be advantageous for evaluating DAI. It provides additional and useful information that can help improve the detection, evaluation, treatment and management of patients with DAI [5, 8, 19].

SWI in fact could also help distinguish the various stages of hemorrhage. There exist 5 distinct stages of hemorrhage [13]:

- Hyperacute – This includes the intracellular oxyhemoglobin and is characterized by a long T1 and T2.

- Acute – This includes the intracellular deoxyhemoglobin which is characterized by a long T1 and short T2.
- Early subacute - This includes intracellular methemoglobin which has a short T1 and long T2.

Late subacute – This includes extracellular Their appearance on SWI depends on whether the species are paramagnetic or not. The 'heme' iron undergoes oxidative denaturation when the hemoglobin is not exposed to high oxygen concentrations, resulting in the formation of methemoglobin. Deoxyhemoglobin, methemoglobin, ferritin and hemosiderin are paramagnetic in nature and because of their relative short T2 rates, they can be visible on SWI [5, 19]. Also, because of their varying T2 values, the different stages of hemorrhagic lesions could be identified based on the degree of hypointensity. No SWI related studies have been done so far to help identify the various stages. Also, other aspects of TBI could be researched with the help of SWI and other MR sequences like FLAIR, DTI etc. Efficient and effective evaluation of TBI could be done by looking at the hemorrhagic as well as the non-hemorrhagic lesions. One could also research to see if every hemorrhagic lesion is associated with a non-hemorrhagic lesion [1].

- Studies have proven that SWI is capable of identifying more lesions than conventional MR imaging techniques and CT scans. One could generate scoring reports methemoglobin which has a short T1 and T2.
- Chronic – This includes break down products ferritin and hemosiderin which is characterized by a short T2.

based on lesion number, size, volume, location, Glasgow Coma Scale, etc that could help in efficient diagnosis, prognosis, proper treatment planning and hopefully a better correlation with outcome.

3.3.2 Cerebral Stroke

Cerebral stroke occurs when the blood supply to the brain is abruptly interrupted or when blood vessels in the brain rupture resulting in a blood spill. It can be classified into ischemic and hemorrhagic stroke. Intracerebral hemorrhage (ICH) is a feared complication of stroke. At present, CT is considered as the gold standard when compared to other modalities. But in some cases like in that of TBI, micro bleeds, petechial blood products caused by ischemic infarction are undetected. SWI could prove to be a powerful technique to diagnose and assess ICH as well [8, 10, 11, 12].

In the case of stroke, it is necessary to identify hematoma and hemorrhages. Hematoma contains a few products of hemorrhage, hence expresses susceptibility effects and so can be detected. The hyperacute phase in stroke refers to the onset of hemorrhage. They predominantly include intact oxygenated red blood cells which as described earlier is diamagnetic. Lesions are classified to have a center, periphery and an adjoining rim. The center is apparently visible on SWI as hyperintensified regions. The periphery is manifested as hypointensified regions and is seen to circumscribe the center. In the acute phase, deoxygenation occurs from the edge of the hematoma progressing inwards [8]. This results in susceptibility effects owing to the paramagnetism thereby making it visible a hypointensified structures on the SWI.

Also, ischemic stroke could be identified by administering a paramagnetic contrast dye into the arterial circulation. SWI images could be obtained before the administration of the dye and after. Subtraction of the resultant SWI images would result in a high resolution arterial map which would also result in the manifestation of the emboli and/or thrombosis.

3.3.3 Brain Tumor

Cerebral metastasis is a common type of tumor in adults and occurs in about 15-25% in all tumor cases [16]. These spread to the brain mainly via the arterial circulation. Detection of these lesions is necessary for surgical removal or radiation therapy based on the size and location. Though no arterial blood or metastasis is paramagnetic in nature, on administration of a paramagnetic contrast agent, these could be identified. This could be done on comparing or subtracting SWI images after and before injecting the dye.

Tumors tend to develop vasculature around it within which hemorrhages could occur. Owing to SWI's excellent resolution, these could be easily detected and evaluated. Currently, CT scans are used to detect the same [8].

3.3.4 Neurodegenerative Disorders

Some neurodegenerative diseases are characterized by an increase in iron levels in the brain. Iron in fact is the most abundant paramagnetic entity in the brain. Both forms of iron, 'heme' and 'non-heme' contribute to the susceptibility effects. In the case of Hallervorden-Spatz disease, there exists an accumulation of iron-containing pigment in the globus pallidus and substantia nigra. SWI could help evaluate this disorder by

quantizing the iron content in the regions of interest. Other diseases which reflect abnormal ‘heme’ and ‘non-heme’ levels include Parkinson’s disease, Alzheimer’s disease, Huntington Disease, Multiple sclerosis, Down syndrome, thallasemia etc. Once one identifies the regions typical to a disorder where there occurs an increase in the iron content in tissues, SWI could be used to evaluate the condition based on the stage, severity, etc

SWI need not be restricted to the brain. Images could be obtained from other regions too and aid in diagnosis and evaluation [8, 18].

CHAPTER 4

FUTURE WORK

Susceptibility Weighted Imaging is a fairly new imaging technique and has tremendous scope. Its applications can extend to various clinical areas as long as there occurs a susceptibility difference between tissues. Future work could include developing a rich user interface for the reconstruction of SWI which allows the user to set the filter mask size as well as the multiplication factor. Provisions could also be made to incorporate SWI reconstruction from various coils. Also, since the main line of focus is DAI, a semi automated tool for lesion detection and quantization could be built which would help in the better evaluation of DAI and also in the generation of a scoring report which describes the number, volume and location of lesions in the brain. The minimum intensity projection was performed using AFNI. While this does an effective processing, alternate tools could be used for the same. The post processing systems of the Siemens Scanner-Leonardo as well as the post processing console for the CT scanner - Vitrea could be used to analyze the images because of its rich User Interface and exquisite tools which will help in easy counting of lesions.

Currently, SWI could not be processed using the phased array coil. This issue could be solved by implementing an algorithm to extract the real and imaginary images from each individual coil element and accordingly calculating the composite real and imaginary images. Individual images from each array in the coil can be obtained by

modifying the CV while setting up the SWI sequence. Being able to reconstruct SWI using the phased array coil is beneficiary because of the better SNR of the coil. Also, the SWI sequence needs to be optimized. The TE value should be halved to around 20msec or lesser and other sequence parameters need to be carefully determined.

APPENDIX A

SWI IMAGE RECONSTRUCTION PSUEDOCODE

```
%*********************************************************************
**********************************************************************
%
%  UT SOUTHWESTERN MEDICAL CENTER at DALLAS
%  Dept. Of Radiology
%  Author          : Nandita Shetty
%  File name       : MRswi.m
%  Created         : June 24th 2005
%  Software        : MATLAB
%  Version         : 1.2
%  Research title : Evaluation of Diffuse Axonal injury in
%                   Susceptibility Weighted Imaging
% Description     : This file constructs the Susceptibility Weighted
%Images. First, the K space data is reconstructed from the real and
%imaginary images. An effectively high pass filtered image is obtained
%whose phase is used to create the Negative Phase Mask. Multiply the
%(phase mask^m)and the Magnitude Image to create the SWI.
%
%*********************************************************************
**********************************************************************

%INITIALIZE THE IMAGE ARRAYS TO ZERO. THE ARRAY REPRESENTS THE MATRIX
SIZE OF 512X512 PIXELS AND 56 SLICES
Create a matrix of size 512x512x56 for the real images
Create a matrix of size 512x512x56 for the imaginary images
Create a matrix of size 512x512x56 for the magnitude images
Create a matrix of size 512x512x56 for the complex images
Create a matrix of size 512x512x56 for the k space images
Create a matrix of size 512x512x56 for the low pass filtered k space
images
Create a matrix of size 512x512x56 for the high pass filtered complex
images
Create a matrix of size 512x512x56 for the negative phase mask
Create a matrix of size 512x512x56 for the Susceptibility Weighted
images



%READ IMAGE DATA FROM THE DICOM FILES
Open and Read the DICOM info and the 56 slices of the Real, Imaginary
and Magnitude Images



% GENERATE THE COMPLEX IMAGE DATA FROM THE REAL AND IMAGINARY IMAGES
```

Construct the complex data for the entire brain from the 56 real and imaginary images
Reconstruct the Phase Images from the real and imaginary images to test if phase values lie between –pi to +pi

% GENERATE THE K SPACE DATA FROM THE COMPLEX IMAGES
Convert the complex data to type 'double' to perform mathematical operations
Perform a 2D FFT on the complex data
Shift the zero frequency component of the Fourier Transformed image to the center of the spectrum to construct the k space data

% ONCE THE K SPACE DATA IS OBTAINED, APPLY A 2D LOW-PASS HANNING FILTER OF DESIRED MASK SIZE TO ELIMINATE THE LOW SPATIAL FREQUENCY PHASE VARIATION. GENERATE AN N POINT K- SPACE FILTER WHICH IS A N*N FILTER IN 2D.
Set the Hanning filter order
Design the 2D Hanning Filter in Spatial Domain
Convert the spatial domain filter to a frequency domain filter and obtain the frequency response
Implement the low pass filter by multiplying the frequency response with the k space data (which is in the frequency domain)

% EFFECTIVE HIGH PASS FILTERING
Convert the filtered k space data in fourier space to spatial domain by performing an Inverse 2D FFT
Divide the complex data with the low pass filtered k space data to generate an effective high pass data

% CONSTRUCT THE NEGATIVE PHASE MASK WITH VALUES RANGING FROM 0 TO 1
Calculate the phase value for each pixel from the high pass filtered image. Check to see if the phase values lie between –pi to +pi
The negative phase mask is obtained using f(x) = (p(x) + pi)/pi for p(x)<0 and f(x)=0 for p(x)>=0, where p(x) is the phase in radians at x.

% ENHANCE MAGNITUDE CONTRAST TO GENERATE THE SUSCEPTIBILITY WEIGHTED IMAGES WITH WELL DEFINED HYPO-INTENSIFIED REGIONS
Multiply the phase mask 'm' number of times where 'm' represents the multiplication factor
Each magnified phase mask is multiplied with its corresponding magnitude image to generate the Susceptibility Weighted Image
Save the SWI images in 'raw format'

REFERENCES

[1] Haacke M, Xu Y, Cheng Y, Reichenbach J, "Susceptibility weighted Imaging", Magnetic Resonance in Medicine 2004 52:612–618

[2] Reichenbach J, Barth M, Klarhofer M, Kaiser W, Moser E, "High Resolution MR Venography at 3.0 Tesla", Journal of Computed Assisted Tomography 2000 24(6): 949-957

[3] Reichenbach J, Haacke M, "High-resolution BOLD venographic imaging : a window into brain function", NMR in Biomedicine NMR Biomed 2001:14:453-467

[4] Cho Z, Ro Y, Lim T, "NMR Venography Using the susceptibility effect produced by deoxyhemoglobin," Magnetic Resonance in Medicine 1992 28(1):25-38

[5] Tong K, Ashwal S, Holshouser B, Shutter L, Herigault G, Haacke M, Kido D. "Hemorrhagic Shearing Lesions in Children and Adolescents with Posttraumatic Diffuse Axonal Injury: Improved Detection and Initial Results", Radiology 2003 227: 332-339

[6] Haacke M, Brown R, Thompson M, Venkatesan R, "Magnetic Resonance Imaging:Physical Principles and Sequence Design", WILLEY-LISS Publication 1999

[7] Abduljalil A, Schmalbrock P, Novak V, Chakeres D, "Enhanced gray and white matter contrast of phase susceptibility-weighted images in ultra-high-field magnetic resonance imaging", Journal of Magnetic Resonance Imaging 2003 18(3):284-290

[8] Seghal V, Delproposto Z, Haacke M, Tong K, Wycliffe N, Kido D, Xu Y, Neelavalli J, Haddar D, Reichenbach J, "Clinical Applications of Neuroimaging With Susceptibility Weighted Imaging", Journal of Magnetic Resonance Imaging 2005 22:439-450

[9] Robson P, Hall L, "Identifying particles in industrial systems using MRI susceptibility artefacts AIChE Journal 2005 51(6):1633-1640

[10] Zaheer A, Ozsunarn Y, Schaefer P, "Magnetic Resonance Imaging of Cerebral Hemorrhagic Stroke", Topics in Magnetic Resonance Imaging 2000 11(5): 288-299

[11] Hermier M, Nighoghossian N, "Contribution of susceptibility weighted imaging to acute stroke assessment", Stroke 2004 Aug 35(8):1989-94

[12] Neumann-Haefelin T, Moseley M, Albers G "New magnetic resonance imaging methods for cerebrovascular disease: Emerging clinical applications", Annals of Neurology 2000 47(5):559-570

[13] Bradley W, "MR Appearance of Hemorrhage in the Brain." Radiology 1993 189:15-26

[14] Rauscher A, Sedlacik J, Markus B, Mentzel J, Reichenbach J, "Magnetic Susceptibility-Weighted MR Phase Imaging of the Human Brain", American Journal of Neuro Radiology 2005 26:736-742

[15] Wang Y, Yu Y, Li D, Bae K, Brown J, Lin W, Haacke M, "Artery and vein separation using susceptibility-dependent phase in contrast-enhanced MRA ", Journal of Magnetic Resonance Imaging 2000 12(5):661-670

[16] Essig M, Waschkies M, Wenz F, Debus J, Hentrich H, Knopp M, "Assessment of Brain Metastases with Dynamic Susceptibility-Weighted Contrast-enhanced MR Imaging: Initial Results" Radiology 2003 228:193-199.

[17] Law M, Oh S, Babb J, Wang E, Inglese M, Zagzag D, Knopp E, Johnson G, "Low Grade Gliomas: Dynamic Susceptibility-Weighted Contrast-enhanced Perfusion MR Imaging-Prediction of Patient Clinical Response. Radiology 2006 238:658-667

[18] Vymazal J, Brooks R, Patronas N, Hajek M, Bulte J, Di Chiro G, "Magnetic Resonance Imaging of Brain Iron in Health and Disease", Journal of the Neurological Sciences 1995 134:19-26

[19] Tong K, Ashwal S, Holshouser B, Nickerson J, Wall C, Shutter L, Osterdock R, Haacke M, Kido D, "Diffuse axonal injury in children: Clinical correlation with hemorrhagic lesions", Annals of Neurology 2004 56(1):36-50

[20] Reichenbach J, Venkatesan R, Schillinger d, Kido D, Haacke M, "Small Vessels in the Human Brain : MR Venography with Deoxyhemoglobin as an Intrinsic Contrast Agent", Radiology 1997 204:272-277

[21] Reichenbach J, Mentzel J, Fitzek C, Haacke M, Kido D, Lee b, Kaiser W, "High-Resolution blood oxygen-level dependent MR Venography (HRBV): a new technique" Neuroradiology 2001 43:364-369

[22] Stanberry L, University of Washington, Department of Statistics, fMRI Seminar "Brief Introduction to Functional MRI Data"

[23] Wikipedia – *The Free Encyclopedia*, http://en.wikipedia.org/wiki/Hemoglobin

BIOGRAPHICAL INFORMATION

Nandita R. Shetty received her Bachelor of Engineering degree in Medical Electronics from the Visweswariah Technological University in 2002 and is a rank holder. She worked for Philips Medical Systems, the MR group as a software developer for a year and was a part of the System Performance Tool project. She pursued her masters in Bioengineering at The University of Texas at Arlington and at the University of Texas Southwestern Medical Center at Dallas in Spring 2004. Her interests include Medical Imaging and Processing and her area of interest includes Magnetic Resonance Imaging. Effective Summer 2005, she has been appointed as a Graduate Research Assistant in the Advanced Radiology Lab under the supervision of Dr. Michael D. Devous, Sr.